Solar Energy Materials & Solar Cells 133 (2015) 113–118

Contents lists available at ScienceDirect

Solar Energy Materials & Solar Cells

journal homepage: www.elsevier.com/locate/solmat

Accurate extraction of the series resistance of aluminum local back surface field silicon wafer solar cells

Jia Chen [a,b,*], Zhe Ren Du [a,c], Fajun Ma [a,c], Fen Lin [a], Debajyoti Sarangi [a], Bram Hoex [a], Armin G. Aberle [a,b,c]

[a] Solar Energy Research Institute of Singapore, National University of Singapore, Singapore
[b] NUS Graduate School for Integrative Sciences and Engineering, National University of Singapore, Singapore
[c] Department of Electrical and Computer Engineering, National University of Singapore, Singapore

ARTICLE INFO

Article history:
Received 7 April 2014
Received in revised form
20 August 2014
Accepted 3 October 2014

Keywords:
Al-LBSF
Silicon solar cells
Series resistance

ABSTRACT

Aluminum local back surface field (Al-LBSF) silicon wafer solar cells are currently intensively investigated in the photovoltaic community and are expected to enter mass production in the near future. In this work we show that this solar cell architecture can pose significant challenges in the determination of the series resistance at the maximum power point. We also show that some of the traditional methods for extracting the series resistance of these cells result in a severe underestimation, due to injection dependent saturation current densities. By using a combination of electro- and photo-luminescence images, we demonstrate that the series resistance of Al-LBSF solar cells can be accurately determined.

1. Introduction

The silicon (Si) wafer based sector of the photovoltaic (PV) industry is trying to reduce costs by increasing the solar cell efficiency of increasingly thinner Si wafers. A standard full-area Al back surface field (Al-BSF) provides only a moderate level of electronic passivation of the rear surface. With significantly improved rear passivation at a relatively low additional cost, solar cells with an Al local back surface field (Al-LBSF) [1] are of great interest. However several issues were observed for screen-printed Al-LBSF solar cells, such as thin p^+ layers within the rear contacted regions [2] and the formation of voids between the Si substrate and the Al rear contact [3,4]. A large series resistance R_s can be observed for this type of solar cell due to the fact that the majority charge carriers need to travel laterally to the rear electrode for collection and, in addition, the contact resistance at the rear is generally higher compared to a full-area Al back surface field (Al-BSF) [5].

Therefore, it is important to accurately extract R_s to characterize and improve the efficiency of Al-LBSF solar cells. Due to the distributed nature of R_s [6–8] it is a function of both voltage and current [9,10]. The current path within the emitter alters when the external conditions change. The R_s of a solar cell can thus be significantly different in dark or under illumination [11]. The series resistance at standard operating condition, $R_{s,lightMPP}$, is the most important parameter to consider as this quantifies the effect of R_s on the solar cell efficiency. The standard operating condition for a terrestrial solar cell refers to the maximum power point (MPP) under AM1.5G illumination at 25 °C cell temperature. The use of $R_{s,lightMPP}$ in advanced fill factor [12] and power loss analyses [13] is also helpful for identifying fabrication issues and improving the efficiency of Al-LBSF solar cells.

In this work, multicrystalline Al-LBSF solar cells were fabricated and their $R_{s,lightMPP}$ was determined using conventional methods [14]: comparison of dark and 1-Sun light I–V measurements (DIV–LIV method) [10], comparison of one-Sun light I–V and J_{sc}–V_{oc} measurements (J_{sc}–V_{oc} method) [10,15], fill factor method [16], and a combination of electro- and photo-luminescence imaging measurements ($R_{s\text{-}PL}$ method) [17]. The comparison of light I–V curves under different illumination levels (double-light method) [15] was not available in this work due to limitations of our I–V tester. We observed a significant underestimation of $R_{s,lightMPP}$ (due to the strongly injection level dependent saturation current densities J_{01} and J_{02}) for the DIV–LIV and J_{sc}–V_{oc} methods. We show that $R_{s,lightMPP}$ can be extracted accurately with the $R_{s\text{-}PL}$ method, as this method extracts $R_{s,lightMPP}$ under operating conditions with a constant bulk injection level. From two-diode simulations and a detailed analysis, it seems that this result is valid not only for Al-LBSF cells but also for other types of solar cells.

2. Experimental setup

A batch of p-type 6 in. wide multicrystalline silicon Al-LBSF solar cells with homogenous n-type emitter was fabricated

* Corresponding author at: Solar Energy Research Institute of Singapore, National University of Singapore, 7 Engineering Drive 1, Block E3A, #06-01, Singapore 117574, Singapore. Tel.: +65 66011677.
E-mail address: a0033548@nus.edu.sg (J. Chen).

http://dx.doi.org/10.1016/j.solmat.2014.10.003
0927-0248/

according to the processing flow of Fig. 1. The wafers were wet-chemically textured on both sides, followed by a phosphorus diffusion of 70 Ω/sq. After wet-chemical edge isolation and phosphosilicate glass (PSG) removal, a 100 nm thick masking layer of silicon nitride (SiN_x) was deposited onto the front surface by plasma-enhanced chemical vapor deposition (PECVD). A chemical solution ('SERIS etch' [18]) developed in our institute was used for rear side polishing. The wafers were then split into three groups. The masking layer of Group C was removed by etching in diluted HF (10%), and a 70 nm SiN_x antireflection coating was deposited onto the front of the wafers. A stack of 40 nm aluminum oxide (AlO_x) and 100 nm SiN_x was then deposited onto the rear of the wafers of all groups. All the dielectric layers were deposited by PECVD in an industrial inline deposition system (SiNA-XS, Roth & Rau). All groups were completed into full solar cells with optimized laser-opened line contacts (100 μm wide lines with a pitch of 1.0 mm [19–21]). For the laser processing step, a laser with picosecond pulses (duration ~10 ps, wavelength 532 nm) was used (Super Rapid, Lumera). Solar cells of Group A received a short KOH dip (10%, 70 °C) after laser ablation to remove possible laser damage [19]. Cells from all groups were then fired in an industrial belt fast firing furnace (Ultraflex, Despatch Industries) with a set peak temperature of 800 °C. For reference purposes, standard full-area Al-BSF solar cells were also fabricated in this experiment. Upon completion of all solar cells, the 1-Sun and dark current–voltage characteristics were measured under standard testing conditions (Solsim 210, Aescusoft). The solar cells were also analyzed with the Suns–V_{oc} method (Sinton, WCT-120).

From the measured data, $R_{s,lightMPP}$ was determined using the DIV–LIV, J_{sc}–V_{oc}, and *FF* methods. The $R_{s,lightMPP}$ was also extracted from a combination of electro- and photo-luminescence imaging measurements (LIS-R1, BT Imaging) [17]. One cell from every group was selected for a detailed analysis of the measured *I–V* characteristics using the two-diode model. Finally the effective minority carrier lifetime τ_{eff} of the solar cells was extracted from Suns–V_{oc} measurements (Suns–V_{oc}, Sinton Instruments).

3. Experimental results and discussion

3.1. Solar cell results

The measured 1-Sun *I–V* parameters of the investigated multi-Si Al-LBSF solar cells are listed in Table 1. Two cells from each group were selected for investigation. Cells from Group C have a higher open-circuit voltage (V_{oc}), fill factor (*FF*) and efficiency (*eff*) due to their better front surface passivation. The front SiN_x of Group A and Group B cells deteriorated during the step of rear side polishing and KOH etching. The $R_{s,lightMPP}$ of several representative cells from each group was determined using the DIV–LIV, J_{sc}–V_{oc}, *FF* and $R_{S\text{-}PL}$ methods Fig. 2. The $R_{s,lightMPP}$ of the Al-BSF reference cells fabricated in the same batch was determined to be $\sim 0.50 \pm 0.01\ \Omega\,cm^2$, using the DIV–LIV method. Compared to Al-BSF cells, there is an additional series resistance ΔR_s for Al-LBSF cells with an identical front grid, emitter and bulk resistivity. This ΔR_s is due to lateral transport of carriers in the bulk and an increased contact resistance [5,22]. Based on the Fischer–Plagwitz model [5,22], ΔR_s of our LBSF cells is 0.15 $\Omega\,cm^2$. The lower limit of $R_{s,lightMPP}$ of our Al-LBSF cells is thus about 0.65 $\Omega\,cm^2$. As can be seen from Fig. 2 the J_{sc}–V_{oc} method and, particularly, the DIV–LIV method produce a severe underestimation of $R_{s,lightMPP}$ of Al-LBSF cells of Groups A and B. In contrast, for Group C cells all 4 R_s methods are found to give rather consistent results.

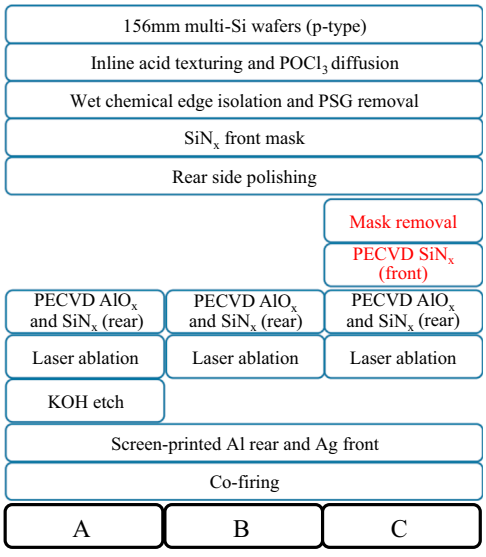

Fig. 1. Fabrication sequence of the investigated Al-LBSF solar cells. The peak temperature during the co-firing step was 800 °C.

3.2. Comparison of different methods for R_s determination

To investigate the differences between the $R_{s,lightMPP}$ values determined by the different methods, we need to discuss these methods and their boundary conditions in more detail. In the DIV–LIV method, the J_{sc}-shifted 1-Sun light (LIV) and dark *I–V* curves (DIV) are compared. Assuming constant saturation current densities, and negligible impact of both the shunt and the series resistance in the dark [10], the voltage difference ($\Delta V_{DIV-LIV}$) between these two curves at J_{MPP} can be solely attributed to the 1-Sun series resistance. Using the current at MPP (J_{MPP}), $R_{s,lightMPP}$ at the MPP can be calculated by

$$R_{s,DIV-LIV} = \Delta V_{DIV-LIV}/J_{MPP} \quad (1)$$

The J_{sc}–V_{oc} method is not affected by the impact of the series resistance, as neither J_{sc} nor V_{oc} of reasonably good Si wafer solar

Table 1
Measured one-Sun parameters of the investigated Al-LBSF cells. Two cells from each group were selected.

Cell parameter	Group A		Group B		Group C	
	A1	A2	B1	B2	C1	C2
J_{sc}[mA/cm^2]	35.3	34.9	35.2	35.3	35.6	35.5
V_{oc}[mV]	608	560	608	607	620	620
FF [%]	74.1	69.1	72.3	73.2	76.2	77.2
eff [%]	15.9	13.5	15.5	15.6	16.8	17.0

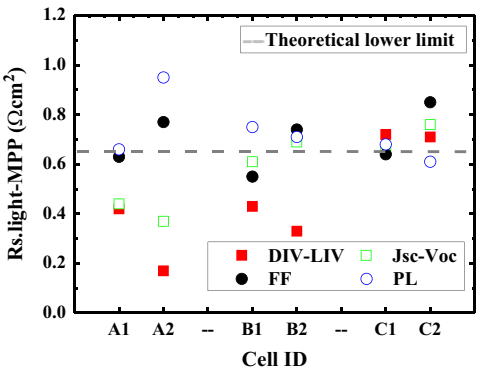

Fig. 2. $R_{s,lightMPP}$ of selected Al-LBSF cells as determined by the DIV–LIV, J_{sc}–V_{oc}, *FF* and $R_{S\text{-}PL}$ methods. The dashed line is the theoretical lower limit of the Al-LBSF cells expected from the Al-BSF reference cells and the Fischer–Plagwitz model.

cells is affected by the R_s. Similarly, a voltage difference ($\Delta V_{J_{sc}-V_{oc}}$) at MPP between its J_{sc}-shifted 1-Sun I–V curve and J_{sc}–V_{oc} curve can be observed. $R_{s,lightMPP}$ is then calculated by

$$R_{s,J_{sc}-V_{oc}} = \Delta V_{J_{sc}-V_{oc}}/J_{MPP} \quad (2)$$

The fill factor (FF) method [16] calculates $R_{s,lightMPP}$ by

$$R_{s,FF} = V_{oc}/J_{sc}(1 - FF/pFF) \quad (3)$$

where V_{oc}, J_{sc} and FF are obtained from the 1-Sun I–V curve and the pseudo-fill factor pFF from the J_{sc}–V_{oc} measurement. This equation is accurate if the following two conditions are satisfied:

$$V_{oc}/nV_T \geq 10 \quad (4)$$

$$R_{s,FF}I_{sc}/V_{oc} \leq 0.4 \quad (5)$$

Eqs. (4) and (5) were satisfied for all the cells used in this work.

The DIV–LIV, J_{sc}–V_{oc} and double-light methods are currently routinely used in both labs and the PV industry to extract the $R_{s,lightMPP}$ of a solar cell. However for practical solar cells the underlying assumptions of these methods are not always strictly satisfied, which will result in some errors. For example the derivation of the DIV–LIV method assumes that the series resistance in the dark ($R_{s,dark}$) has a negligible impact on the DIV curve at V_{MPP}, as the current density at this operating point is relatively low. However it has been shown that this assumption is not necessarily true for a typical industrial silicon wafer solar cell, resulting in a 5% overestimation of $R_{s,lightMPP}$ [23]. By considering the impact of the $R_{s,dark}$, a more accurate estimation of $R_{s,lightMPP}$ can be obtained [24]. The DIV–LIV and J_{sc}–V_{oc} methods assume constant J_{01} and J_{02} under different illuminations. However, if the J_{01} and J_{02} values are injection level dependent, it has been shown that the J_{sc}–V_{oc} method strongly underestimates $R_{s,lightMPP}$ [10]. Similarly, an underestimation of $R_{s,lightMPP}$ is reported for PERC (passivated emitter rear contact) solar cells with injection-dependent τ_{eff} values [9,25]. Injection-dependent τ_{eff}, J_{01} and J_{02} can, for example, be caused by B–O complexes [26] or, in the case of PERL-type cells (passivated emitter rear locally diffused), an injection-dependent rear surface recombination velocity [10,27,28].

The DIV–LIV and J_{sc}–V_{oc} methods both underestimate $R_{s,lightMPP}$ when the solar cell has injection level dependent saturation current densities. To find $R_{s,lightMPP}$ accurately for such solar cells it is important to find a method that extracts the series resistance from operating conditions with identical injection levels, such as the $R_{s\text{-}PL}$ method. In this method, the series resistance image of the solar cell is extracted using a combination of electro- and photo-luminescence images. The global $R_{s,PL}$ of the whole solar cell is calculated from the arithmetic mean value of the series resistance of each pixel [29]. A very high local series resistance in a small area of the cell could lead to error in estimation of the global series resistance [30]. The resulting series resistance images of three Al-LBSF solar cells are shown in Fig. 3.

The key assumption of the $R_{s\text{-}PL}$ method presented by Kampwerth et al. [17] is to choose two different solar cell operating points with the same luminescence intensity. The luminescence intensity of every point of the solar cell, $I_{camera,i}$, can be expressed as [17,31]

$$I_{camera,i} = C_i \exp(eU_i/kT) + C_{offset} \quad (6)$$

where C_i is the correlation constant of local diode voltage and luminescence intensity, C_{offset} is the junction voltage independent offset of the luminescence signal caused by radiative recombination of diffusion-limited carriers, U_i is the local diode voltage [17], e is the electron charge, k the Boltzmann constant and T the absolute temperature. From Eq. (6), the same luminescence intensity ensures an identical local diode voltage for the two operating points. The conversion of luminescence intensity into absolute voltages and assumptions about dark current densities are not required anymore [17]. The series resistance $R_{s,xy}$ of each pixel can thus be calculated by

$$R_{s,xy} = -\Delta U_{term}/\Delta J \quad (7)$$

where ΔU_{term} is the difference of the terminal voltages and ΔJ is the difference of the short-circuit current densities of the two points. The short-circuit current density is assumed to be approximately constant over the cell. As a method similar to $R_{s\text{-}PL}$, the coupled determination of dark saturation current and series resistance (C-DCR) [32] may also be used to extracted accurate $R_{s,lightMPP}$.

3.3. Injection dependent dark saturation current densities

To investigate the root cause of the underestimation of $R_{s,lightMPP}$ in our LBSF cells, one cell from every group was selected for a detailed study of their I–V characteristics. Their measured DIV and one-Sun LIV curves are plotted in Fig. 4. The experimental DIV, 1-Sun LIV and J_{sc}–V_{oc} of the three cells could all be fitted very well by the two-diode

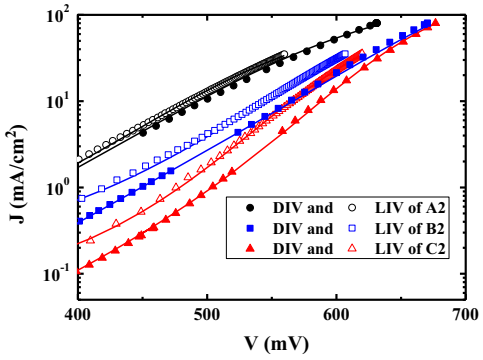

Fig. 4. Dark and J_{sc}-shifted 1-Sun I–V characteristics of cells A2–C2. The solid lines show two-diode model fits.

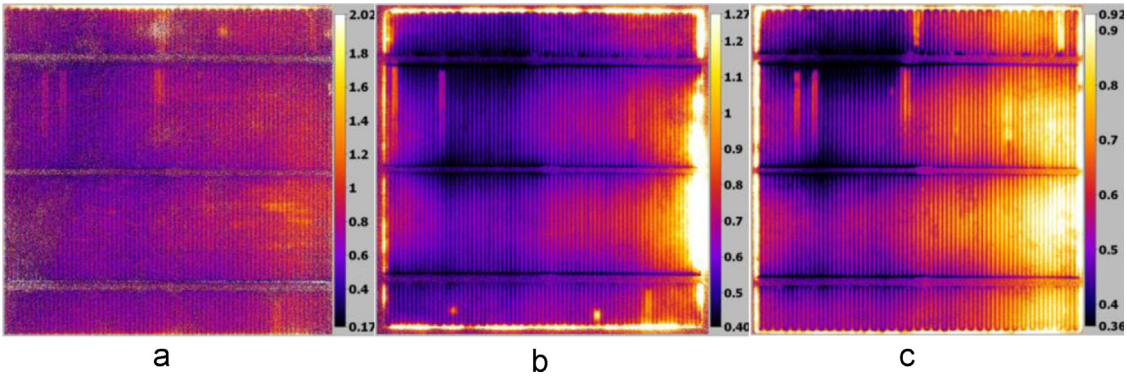

Fig. 3. Luminescence-based series resistance image of Al-LBSF cells.(a) A2, (b) B2 and (c) C2.

Table 2
Parameters used to fit DIV, LIV and J_{sc}–V_{oc} of the cells by two-diode model.

Cell parameter	A2			B2			C2		
	DIV	LIV	J_{sc}–V_{oc}	DIV	LIV	J_{sc}–V_{oc}	DIV	LIV	J_{sc}–V_{oc}
J_{01}[A/cm^2]	7.5×10^{-12}	5.4×10^{-12}	1.6×10^{-12}	1.4×10^{-12}	1.1×10^{-12}	1.1×10^{-12}	8.8×10^{-13}	8.9×10^{-13}	1.5×10^{-12}
J_{02}[A/cm^2]	7.1×10^{-7}	3.1×10^{-7}	8.2×10^{-7}	1.5×10^{-7}	1.2×10^{-7}	1.2×10^{-7}	3.9×10^{-8}	3.1×10^{-8}	3.4×10^{-8}
$R_{s,lightMPP}$[Ω cm^2]	0.82	1.2	0	0.67	0.62	0	0.40	0.82	0
R_{sh}[Ω cm^2]	2.0×10^{4}	2.2×10^{4}	1.1×10^{5}	3.5×10^{4}	2.4×10^{4}	1.7×10^{4}	3.6×10^{4}	1.2×10^{5}	6.9×10^{4}

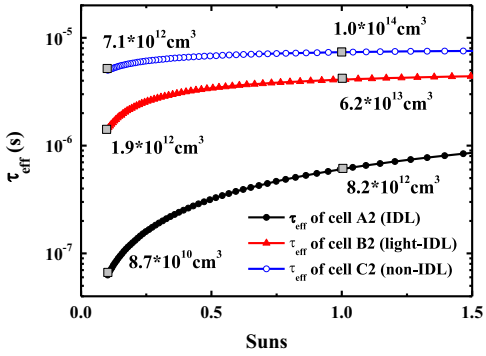

Fig. 5. Effective lifetime of three Al-LBSF solar cells as a function of the light intensity (extracted from Suns–V_{oc} measurements). IDL stands for injection-dependent lifetime.

Table 3
Solar cell parameters used in the simulations of Fig. 6.

J_{ph}[mA/cm^2]	R_s[Ω cm^2]	R_{sh}[Ω cm^2]	J_{01}[A/cm^2]	J_{02}[A/cm^2]
37	0.5	10^4	10^{-6}–10^{-15}	10^{-6}–10^{-11}

model (Fig. 4). The fit parameters for the 3 solar cells shown in Fig. 4 are listed in Table 2. As can be seen, the J_{01} and J_{02} of cell A2 are significantly lower at one-Sun illumination than in the dark.

In Fig. 5 the effective lifetime τ_{eff} of the solar cells is plotted as a function of the light intensity as derived from Suns–V_{oc} measurements. The τ_{eff} of cell A2 is one order of magnitude higher at 1 Sun compared to the value at 0.1 Sun. In contrast the τ_{eff} of cells B2 and, particularly, C2 is only weakly dependent on the illumination intensity. There appears to be a strong correlation between the injection level dependence of τ_{eff} and the accuracy of the $R_{s,lightMPP}$ values determined with the DIV–LIV method and the J_{sc}–V_{oc} method. In the next section we will investigate this correlation in more detail.

3.4. Two-diode simulation

The solar cells' *I–V* characteristics were simulated using the two-diode model. This model includes a current source supplying a photo-generated current J_{ph} and two diodes with dark saturation current densities J_{01} and J_{02} and ideality factors 1 and 2, respectively. A series resistance R_s and a shunt resistance R_{sh} are also included in the circuit. It is reported that some types of solar cells can be simulated more accurately by a three-diode model or a two-diode model with different ideality factors [33]. However, the main results of this paper are not affected by the equivalent circuit model used for the simulations. The parameters used for the solar cell simulations are summarized in Table 3. Due to its distributed nature, it is most accurate to simulate the R_s of the cell as a function of voltage and illumination. However, as this dependence varies with the solar cell structure and processing, a constant R_s was adopted to simplify the analysis.

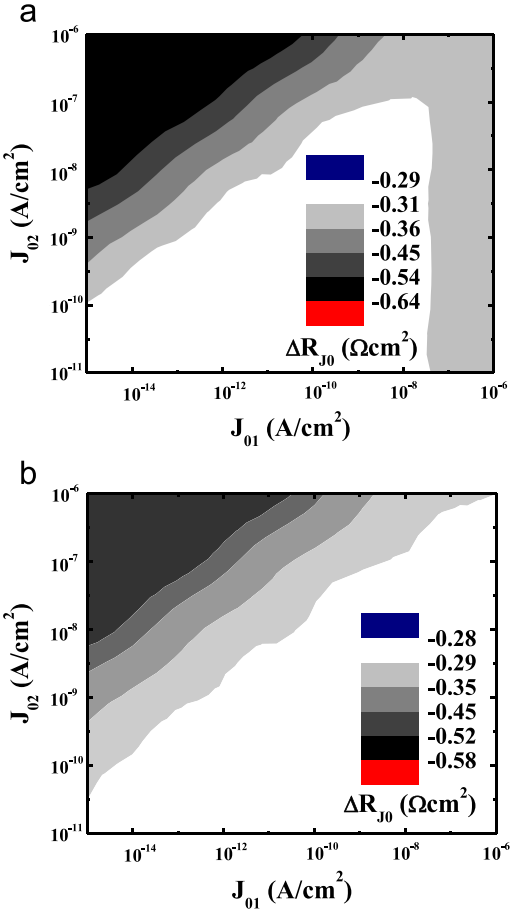

Fig. 6. $R_{s,lightMPP}$ error caused by injection-dependent J_{01} and J_{02} when (a) using the DIV–LIV method. In dark the J_{01} and J_{02} values are assumed to be 1.5 times higher than that under 1-Sun illumination and (b) using the J_{sc}–V_{oc} method. J_{01} and J_{02} were assumed to increase linearly as a function of the light intensity from their value at 0 Sun to their value at 1 Sun.

Using the parameters, *I–V* curves (1-Sun LIV, J_{sc}–V_{oc} and DIV) of the solar cell were simulated. $R_{s,lightMPP}$ was then calculated from the simulated *I–V* characteristics. The error of $R_{s,lightMPP}$ due to injection dependent J_{01} and J_{02}, ΔR_{J0}, was determined by comparing the user-defined R_s value and the calculated $R_{s,lightMPP}$ value. We assume that the J_{01} and J_{02} values in dark are 1.5 times higher than the J_{01} and J_{02} values under 1-Sun illumination, which is similar to the case of the Group A cells. For the simulated J_{sc}–V_{oc} curves J_{01} and J_{02} were assumed to increase linearly as a function of the light intensity from their value at 0 Sun to their value at 1 Sun. Fig. 6 shows the R_s error caused by the injection-dependent J_{01} and J_{02} using (a) DIV–LIV and (b) J_{sc}–V_{oc} methods. As can be seen, a severe underestimation of $R_{s,lightMPP}$ is observed in both methods. This shows that injection-dependent J_{01} and J_{02} values can lead to a very large error (more than 100%) in the extracted $R_{s,lightMPP}$ value. It is highly likely that this effect is the main cause of the observed underestimation of

Table 4
Simulations parameters and extracted R_s for the three types of solar cells. *: In the J_{sc}–V_{oc} simulation of the Group A and Group B solar cells J_0 was assumed to increase linearly as a function of the light intensity from its starting value in the dark.

	Simulation parameters									Calculated R_S	
	J_{ph}[mA/cm^2]	R_s[Ω cm^2]	R_{sh}[Ω cm^2]	LIV		DIV		J_{sc}–V_{oc}		$R_{s-DIV-LIV}$[Ω cm^2]	R_s–J_{sc}–V_{oc}[Ω cm^2]
				J_{01}[A/cm^2]	J_{02}[A/cm^2]	J_{01}[A/cm^2]	J_{02}[A/cm^2]	J_{01}[A/cm^2]	J_{02}[A/cm^2]		
A	35.5	0.65	2×10^4	10^{-12}	10^{-7}	1.5×10^{-12}	1.5×10^{-7}	*		0.16	0.14
B	35.5	0.65	2×10^4	10^{-12}	10^{-7}	1.2×10^{-12}	1.2×10^{-7}			0.47	0.43
C	35.5	0.65	2×10^4	10^{-12}	10^{-7}	10^{-12}	10^{-7}	10^{-12}	10^{-7}	0.71	0.65

$R_{s,lightMPP}$ of Group A cells when using the DIV–LIV and J_{sc}–V_{oc} methods. The Al-LBSF cells from the three groups in the experiment were simulated using the parameters summarized in Table 4. $R_{s,lightMPP}$ values were extracted from the generated I–V curves using the DIV–LIV and J_{sc}–V_{oc} methods. Severe and moderate underestimation of $R_{s,lightMPP}$ was observed for Group A and B cells respectively, which agrees with the experimental observation. It should be noted that this analysis is not limited to Al-LBSF solar cells but is generally valid for all types of solar cells having a strongly injection level dependent bulk lifetime.

4. Conclusion

Accurate determination of the series resistance at standard operating conditions ($R_{s,lightMPP}$) is crucial for the accurate characterization and power loss analysis of any kind of solar cell. The state-of-the-art methods for determining $R_{s,lightMPP}$ are the comparison of dark and 1-Sun I–V measurements (DIV–LIV method), comparison of 1-Sun I–V and J_{sc}–V_{oc} measurements (J_{sc}–V_{oc} method) and comparison of light I–V curves under different illumination levels (double-light method). However, for practical solar cells the underlying assumptions of these methods are not always strictly satisfied. Violation of the assumptions could lead to possible errors.

In this work, three groups of p-type 6 in. multicrystalline silicon Al-LBSF solar cells with homogenous emitter were fabricated. Their $R_{s,lightMPP}$ values were determined using various methods. A severe underestimation of $R_{s,lightMPP}$ was observed for Group A cells when the standard DIV–LIV method and the J_{sc}–V_{oc} method were used. Clear evidence for an injection level dependent saturation current density of Group A cells was found. By means of two-diode simulations we showed that the injection-dependent J_{01} and J_{02} are the most likely cause for the underestimated $R_{s,lightMPP}$ values. We proposed that, by using a combination of electro- and photoluminescence images, the correct $R_{s,lightMPP}$ value can be extracted, as this method intrinsically assumes an identical injection level at the operating points for extraction of $R_{s,lightMPP}$.

Acknowledgment

SERIS is sponsored by the National University of Singapore (NUS) and Singapore's National Research Foundation (NRF) through the Singapore Economic Development Board (EDB). This work was sponsored by NRF grant NRF2009EWT-CERP001-056.

Reference

[1] J. Knobloch, A.G. Aberle, B. Voss, Cost effective processes for silicon solar cells with high performance, in: Proceedings of the 9th European PV Solar Energy Conference, Freiburg, 1989, pp. 777–780.
[2] M. Rauer, R. Woehl, K. Ruhle, C. Schmiga, M. Hermle, M. Horteis, D. Biro, Aluminum alloying in local contact areas on dielectrically passivated rear surfaces of silicon solar cells, IEEE Electron Device Lett. 32 (7) (2011) 916–918.
[3] E. Urrejola, K. Peter, H. Plagwitz, G. Schubert, Silicon diffusion in aluminum for rear passivated solar cells, Appl. Phys. Lett. 98 (2011) 153508.
[4] C. Chen, H.M. Tong, K.N. Tu, Electromigration and thermomigration in Pb-free flip-chip solder joints, Annu. Rev. Mater. Res. 40 (2010) 531–555.
[5] H. Plagwitz Ph.D thesis, University of Hannover, Germany, 2007.
[6] L.D. Nielsen, Distributed series resistance effects in solar cells, IEEE Trans. Electron Devices 29 (1982) 821–827.
[7] G.M. Smirnov, J.E. Mahan, Distributed series resistance in photovoltaic devices; intensity and loading effects, Solid-State Electron. 23 (1980) 1055–1058.
[8] G.L. Araujo, A. Cuevas, J.M. Ruiz, The effect of distributed series resistance on the dark and illuminated current–voltage characteristics of solar cells, IEEE Trans. Electron Devices 33 (1986) 391–401.
[9] P.P. Altermatt, G. Heiser, A.G. Aberle, A.H. Wang, J.H. Zhao, S.J. Robinson, S. Bowden, M.A. Green, Spatially resolved analysis and minimization of resistive losses in high-efficiency Si solar cells, Prog. Photovolt.: Res. Appl. 4 (1996) 399–414.
[10] K.C. Fong, K.R. McIntosh, A.W. Blakers, Accurate series resistance measurement of solar cells, Prog Photovolt. 21 (2011) 490–499.
[11] A.G. Aberle, S.R. Wenham and M.A. Green, A new method for accurate measurement of the lumped series resistance of solar cells, Proceedings of the 23rd IEEE Photovoltaic Specialists Conference, Louisville, 1993, pp. 133–139.
[12] A. Khanna, T. Mueller, R.A. Stangl, B. Hoex, P.K. Basu, A.G. Aberle, A fill factor loss analysis method for silicon wafer solar cells, IEEE J. Photovolt. 3 (4) (2013) 1170–1177.
[13] A.G. Aberle, W. Zhang, B. Hoex, Advanced loss analysis method for silicon wafer solar cells, Energy Procedia 8 (2011) 244–249.
[14] D. Pysch, A. Mette, S.W. Glunz, A review and comparison of different methods to determine the series resistance of solar cells, Sol. Energy Mater. Sol. Cells 91 (2007) 1698–1706.
[15] M. Wolf, H. Rauschenbach, Series resistance effects on solar cell measurements, Adv. Energy Convers. 3 (1963) 455–479.
[16] M.A. Green, Solar cells: Operating Principles, Technology and System Applications, The University of New South Wales, Sydney, Australia (1998) 96.
[17] H. Kampwerth, T. Trupke, J.W. Weber, Y. Augarten, Advanced luminescence based effective series resistance imaging of silicon solar cells, Appl. Phys. Lett. 93 (2008) 202102.
[18] P.K. Basu, Z. Hameiri, D. Sarangi, J. Cunnusamy, E. Carmona, J. Avancena, S. Chakraborty, K.D. Shetty, B. Hoex, M.B. Boreland, Achieving high efficiencies with a low-cost etch for in-line-diffused silicon wafer cells, Photovolt. Int. 19 (2013) 51–56.
[19] Z.R. Du, N. Palina, J. Chen, M.H. Hong, B. Hoex, Rear-side contact opening by laser ablation for industrial screen-printed aluminium local back surface field silicon wafer solar cells, Energy Procedia 25 (2012) 19–27.
[20] Z.R. Du, N. Palina, J. Chen, A.G. Aberle, B. Hoex, M. Hong, Enhancement of laser-induced rear surface spallation by pyramid textured structures on silicon wafer solar cells, Opt. Express 20 (S6) (2012) A984–A990.
[21] J. Chen, Z.H.J. Tey, Z.R. Du, F. Lin, B. Hoex, A.G. Aberle, Investigation of screen-printed rear contacts for aluminum local back surface field silicon wafer solar cells, IEEE J. Photovol. 3 (2) (2013) 690–696.
[22] B. Fischer Ph.D thesis, University of Konstanz, Germany, 2003.
[23] J. Dicker, Ph.D thesis, University of Konstanz, Germany, 2003.
[24] J. Greulich, M. Glatthaar, S. Rein, Separation of series resistance and space charge region recombination in crystalline silicon solar cells from dark and Illuminated current–voltage characteristics, IEEE J. Photovolt. 2 (3) (2012) 241–246.
[25] S. Steingrube, H. Wagner, H. Hannebauer, S. Gatz, R. Chen, S.T. Dunham, T. Dullweber, P.P. Altermatt, R. Brendel, Loss analysis and improvements of industrially fabricated Cz-Si solar cells by means of process and device simulations, Energy Procedia 8 (2011) 263–268.
[26] K. Bothe, R. Sinton, J. Schmidt, Prog. Photovolt. 13 (2005) 287.
[27] A.G. Aberle, S.J. Robinson, A. Wang, J. Zhao, S.R. Wenham, M.A. Green, High-efficiency silicon solar cells: fill factor limitations and non-ideal diode behaviour due to voltage-dependent rear surface recombination velocity, Prog. Photovolt. 1 (1993) 133–143.
[28] S. Steingrube, P.P. Altermatt, D. Zielke, F. Werner, J. Schmidt, R. Brendel, Reduced passivation of silicon surfaces at low injection densities caused by H-induced defects, Proceedings of the 25th EU PV Solar Energy Conference, Valencia, 2010, pp. 1748–1754.

[29] K. Ramspeck, K. Bothe, D. Hinken, B. Fischer, J. Schmidt, R. Brendel, Recombination current and series resistance imaging of solar cells by combined luminescence and lock-in thermography, App. Phys. Lett. 90 (2007) 153502.
[30] H. Höffler, J. Haunschild, R. Zeidler, S. Rein, Statistical evaluation of a luminescence-based method for imaging the series resistance of solar cells, Energy Procedia 27 (2012) 253–258.
[31] K. Schick, E. Daub, S. Finkbeiner, P. Würfel, Verification of a generalized Planck law for luminescence radiation from silicon solar cells,, Appl. Phys. A: Solids Surf. 54 (109) (1992) 109–114.
[32] B. Michl, M. Kasemann, J. Giesecke, M. Glatthaar, A. Schütt, J. Carstensen, H. Föll, S. Rein, W. Warta, and H. Nagel, Application of luminescence imaging based series resistance measurement methods in an industrial environment, in: Proceedings of the 23rd EUPVSEC, Valencia, 2008, pp. 1176-1181.
[33] K. McIntosh Ph.D thesis, University of New South Wales, Australia, 2001.